https://doi.org/10.48048/tis.2024.7867

Influence of Anode Diffusion Layer on the Performance of a Passive Direct Ethanol Fuel Cell

Panuwat Ekdharmasuit

Faculty of Science Energy and Environment, King Mongkut's University of Technology North Bangkok, Rayong Campus, Rayong 21120, Thailand

(Corresponding author's e-mail: panuwat.e@sciee.kmutnb.ac.th)

Received: 20 December 2023, Revised: 28 January 2024, Accepted: 4 February 2024, Published: 20 May 2024

Abstract

One of the main challenges with passive direct ethanol fuel cells (DEFCs) is ethanol transport management since the liquid ethanol is supplied to the anode compartment by natural processes including convection and diffusion with a low cell operating condition. The significant layer in the cell is the diffusion layer (DL), which facilitates reactants to reach the anode catalyst layer (CL). In this study, the impact of various DLs fabricated of readily accessible commercial materials on cell performance in passive DEFCs with different ethanol feed concentrations was examined with various in-situ characterization methods. The results demonstrate that the cell with a DL coated by the hydrophobic microporous layer (MPL) yielded the best performance of 0.887 $mW \cdot cm^{-2}$ at the optimal ethanol feed concentration of 5 M. In conclusion, the benefits of enhancing ethanol mass transfer to the anode CL would outweigh the drawbacks of preventing ethanol crossover to the cathode.

Keywords: Direct ethanol fuel cell (DEFC), Passive fuel cell, Diffusion layer (DL), Microporous layer (MPL), Electrochemical impedance spectroscopy (EIS)

Abbreviations and acronyms:

BL: Backing Layer
CL: Catalyst Later
CC: Carbon Cloth
CE: Counter Electrode
CP: Carbon Paper
DAFC: Direct Alcohol Fuel Cell
DEFC: Direct Ethanol Fuel Cell
DEGFC: Direct Ethylene Glycol Fuel Cell
DHE: Dynamic Hydrogen Electrode
DMFC: Direct Methanol Fuel Cell
DL: Diffusion Layer
EIS: Electrochemical Impedance Spectroscopy
GDE: Gas Diffusion Electrode
MEA: Membrane Electrode Assembly
MPL: Micro Porous Layer
OCV: Open Circuit Voltage
PEM: Proton Exchange Membrane
PEMFC: Proton Exchange Membrane Fuel Cell
PTFE: Polytetrafluoroethylene
RE: Reference Electrode
WE: Working Electrode

Introduction

Fuel cells (FCs) are devices that directly transform the chemical energy of fuel into electrical energy. They can employ various fuels, including hydrogen gas and many options of liquid fuels. FCs that function with an acidic electrolyte membrane and use hydrogen as their fuel are referred to as proton exchange membrane fuel cells (PEMFCs). They are acknowledged as a prominent type due to their efficient performance in a wide range of applications. For portable power applications, the direct supply of alcohol to the PEMFCs, known as direct alcohol fuel cells (DAFCs), is becoming increasingly popular because of their more convenient operation, compact design, and greater alcohol energy density [1]. Various alcohol fuels have been investigated for use in DAFCs, including methanol for direct methanol fuel cells (DMFCs), ethanol for direct ethanol fuel cells (DEFCs), ethylene glycol for direct ethylene glycol fuel cells

(DEGFCs), and so forth [2]. In the operational concept of DAFC, there are 2 main methods, an active mode and a passive mode, for supplying fuel and oxidant [3]. The active mode, which operates under strong conditions and generates more power, requires an auxiliary component with external power to deliver the oxidant and fuel to the cell. Nonetheless, it comes with higher costs and lower energy densities for the system. In contrast, the passive mode uses natural forces such as convection and diffusion to supply the fuel and oxidant, with a lower condition resulting in a higher system energy density, a straightforward design, and suitability for portable applications. Particularly in passive mode, DAFCs experience lower cell performances due to the sluggish reaction rates and the challenge of supplying homogeneous reactants to the cell [4]. For effective diffusion to the catalyst, high fuel solution concentrations are required to maintain the distribution and a steady supply of reactants to the cell. However, the main problem with using higher fuel concentrations is found to be fuel crossover and water management. A higher level of fuel concentration will promote the fuel crossover effect resulting in an activation loss at the cathode electrode, while a low level of water, occurring at the anode, will lead to a significant activation loss at the anode electrode. A low amount of water, needed for the anode electrode oxidation reaction, causes water to back diffuse from the cathode across the membrane and reach the anode [5]. Therefore, before commercialization, the primary challenges, such as fuel crossover from the anode to the cathode, fuel concentration optimization, and water management, must be addressed.

It is known that the membrane electrode assembly (MEA), consisting of a membrane, anode/cathode catalyst layers (CLs), and anode/cathode diffusion layers (DLs), is a key factor with a remarkable influence on DAFC performance. Among these components, the DL plays crucial roles in mass transport management, including facilitating reactant access to the active layer, removing products from the CL, and establishing a connection between the CL and the current collector plate. DL structure can be constructed as a double layer consisting of a backing layer (BL) and a microporous layer (MPL) [6]. BL is commonly made of porous carbon-based materials such as carbon papers and carbon cloths due to their porous characteristics, including porosity (influences species transport), surface properties (provide suitable hydrophobicity), and appropriate surface roughness (for managing the attachment and coverage of droplets and bubbles) [7]. MPL is a mixture of carbon powder and a hydrophobic or hydrophilic agent that plays a role in controlling droplet and bubble attachment or coverage on the surface [8]. Therefore, DL can be enhanced using a variety of techniques, such as coating the BL surface with polytetrafluoroethylene (PTFE) or incorporating PTFE into the MPL composition to customize the layer thickness and hydrophobicity.

At present, for a mass transport study involving modifications to the DL in passive DAFCs, extensive research has been conducted based on the passive DMFC. Yuan *et al.* [9] enhanced passive DMFC anode DLs with a graphene-carbon nanotube composite, resulting in improved cell performance attributed to enhanced anode catalyst utilization. Yuan *et al.* [10] developed a double anode DL with a carbon-powder MPL in a passive DMFC to control mass transfer through gradient porosity. Optimal cell performance was attained at a 12 M methanol concentration, with the DL enhancing uniform distribution and gas bubble elimination. Oliveira *et al.* [5] investigated different anode DLs in passive DMFCs at various methanol concentrations. Increasing the carbon cloth thickness improved cell performance by reducing methanol crossover. The cell achieved the highest performance when operating without an MPL at a methanol concentration of 3 M. Ong *et al.* [11] explored different carbon materials, including graphene composites, for anode DLs in passive DMFCs across varying methanol concentrations. They identified that a single cell with a graphene-based DL exhibited the best performance at methanol concentrations up to 3 M, attributed to enhanced electrical conductivity and improved methanol transport. A denser MPL layer was found to be effective in minimizing methanol crossover, allowing for the use of higher methanol concentrations. Boni *et al.* [12] examined the influence of key properties, such as the thickness and porosity of the anode DL, on passive DMFC performance. Their analysis considered various characteristics, including methanol crossover, water crossover, overpotential, and model development. Their findings revealed that increasing both the thickness and porosity of the anode DL led to a rise in overpotential, resulting in reduced cell performance. Braz *et al.* [13] investigated anode DLs with different properties and structures in passive DMFCs through polarization and EIS measurements. The cell using a carbon cloth with an MPL as the anode DL displayed the highest performance, reaching a maximum power density of 3 $mW \cdot cm^{-2}$ with a 5 M methanol concentration. This configuration showed improvements in methanol transport and oxidation rates, along with a reduction in methanol crossover. Alias *et al.* [14] enhanced the anode DL of passive DMFCs by introducing an improved MPL that incorporated titanium dioxide (TiO_2) along with carbon materials such as carbon nanofiber (CNF) and carbon black (CB). This modification led to improved electronic resistance, reduced methanol crossover, and enhanced long-term cell stability.

Recently, direct ethanol fuel cell (DEFC), which is directly fed with an ethanol solution as fuel at the anode and oxygen gas or air at the cathode, holds significant promise as a power source with strong

commercialization potential due to several advantages of the used fuel. Ethanol is considered a desirable fuel for direct-feed fuel cells. It can be easily managed, is non-toxic, possesses a substantial energy density (6,280 $Wh \cdot L^{-1}$), and has the potential to be derived from agricultural biomass containing sugars [15]. Until now, the concept of modifying the anode DL structure as a means of managing mass transport in passive DEFCs has remained unexplored. The impact of anode mass transport on the cell performance of a passive DEFC has never been evaluated, and the hydrophobicity, which is an important property of the DL component, has never been distinctly determined. The crucial parameter affecting mass transfer behavior in passive DEFC has not been identified, which would be beneficial for DL design in passive DEFC. In this regard, the modification concept associated with DL improvement in passive DEFC could be taken from passive DMFCs. However, it has been noted in the literature that the rates of kinetic reactions and crossover through the membrane differ between DMFCs and DEFCs [16,17]. Therefore, it was anticipated that the anode structure would have a different effect on mass transport in a passive DEFC than it would in a passive DMFC. In addition, to assess performance and comprehend the various sources of loss within a DAFC, several effective *in-situ* characterization techniques, which are non-intrusive, have been demonstrated during realistic operation. The polarization curve (VI curve) and power density curve, which are strongly dependent on the operating conditions and the component materials, are typically used to assess and compare the cell performance [1,2,3,18]. Lately, electrochemical impedance spectroscopy (EIS) has been proposed as the most widely used technique for accurately distinguishing the different losses [6,7,13,19-22]. Also, anode polarization has been introduced in a two-electrode configuration with a dynamic hydrogen electrode (DHE) to study the half-cell anode behavior [20,23] and the current variable with time measurement has been suggested to investigate the mass transport behavior [14,24].

In this study, the impact of various DLs fabricated of readily accessible commercial materials on the cell performance was examined in passive DEFCs with various ethanol feed concentrations. Various anode DL structures were developed to achieve the targeted power outputs necessary for passive DEFC applications. Several characterization methods were employed, including full-cell polarization, full-cell EIS, half-cell polarization, and current variation with time measurement.

Materials and methods

MEA and stack fabrication

Anode DL had 2 different layer configurations: Either a single layer with only BL or a double layer with BL and an MPL. In the case of DL with a single layer, BLs were made of commercially available materials including untreated carbon paper (Type A, no wet-proofed, E-TEK) (CP), untreated carbon cloth (Type A, no wet-proofed, E-TEK) (CC_A), and treated carbon cloth (Type A, 5 %wet-proofed, E-TEK) (CC_B). In the double-layer diffusion configuration, the BL consisted of untreated carbon paper (Type A, not wet-proofed, E-TEK), while the MPL layer was divided into 2 types: Hydrophilic and hydrophobic MPL. The hydrophilic MPL contained 20 wt.% Nafion and carbon Vulcan with a loading of 2 $mg \cdot cm^{-2}$, while the hydrophobic MPL composed of 20 wt.% PTFE and carbon Vulcan with loading of 2 $mg \cdot cm^{-2}$. The double-layer structures, comprising BL with hydrophilic and hydrophobic MPLs, are denoted as CC_MPL_A and CC_MPL_B, respectively. The compositions and designations of each anode DL are shown in **Table 1**.

Table 1 Compositions of the materials employed in anode DLs.

DL	Composition		Thickness (mm)
	BL	MPL	
CP	Carbon Paper (with no wet proofing)	-	0.175
CC_A	Carbon Cloth (with no wet proofing)	-	0.185
CC_B	Carbon Cloth (with a standard 5 % weight wet proofing)	-	0.335
CC_MPL_A	Carbon Cloth (with no wet proofing)	Hydrophilic (20 % Nafion ionomer + Vulcan carbon powder)	0.330
CC_MPL_B	Carbon Cloth (with no wet proofing)	Hydrophobic (20 % PTFE + Vulcan carbon powder)	0.331

The anode catalyst slurry was 2 mg·cm^{-2} Pt-Sn/C (3:1 a/o of Pt:Sn, supplied by Johnson Matthey) mixed with a Nafion ionomer (20 wt.% of the dry CL, supplied by Fuel Cell Store). The anode CL was made by applying the slurry onto the anode MPL and then performing the dry process for an hour at 80 °C in the oven. The cathode electrode was a commercial gas diffusion electrode (GDE) with 0.5 mg Pt·cm^{-2} on Vulcan XC-72 carbon powder (0.835 mm thick carbon cloth construction, E-LAT®, E-TEK). Each side featured an active surface area of 5 m^2, and the experiment employed Nafion® 115 (supplied by Dupont) as a proton exchange membrane (PEM). The membrane preparation involved 3 key stages at a constant 70 °C for 1 h each: Cleaning with 3 % H_2O_2, boiling in 0.5 M H_2SO_4, and rinsing with de-ionized water. The MEA included anode and cathode electrodes on both sides of the Nafion membrane, as depicted in **Figure 1**. Finally, the MEA was compressed between 2 stainless steel current collectors and 2 acrylic blocks to create the custom-made single-cell stack, as illustrated in **Figure 2**.

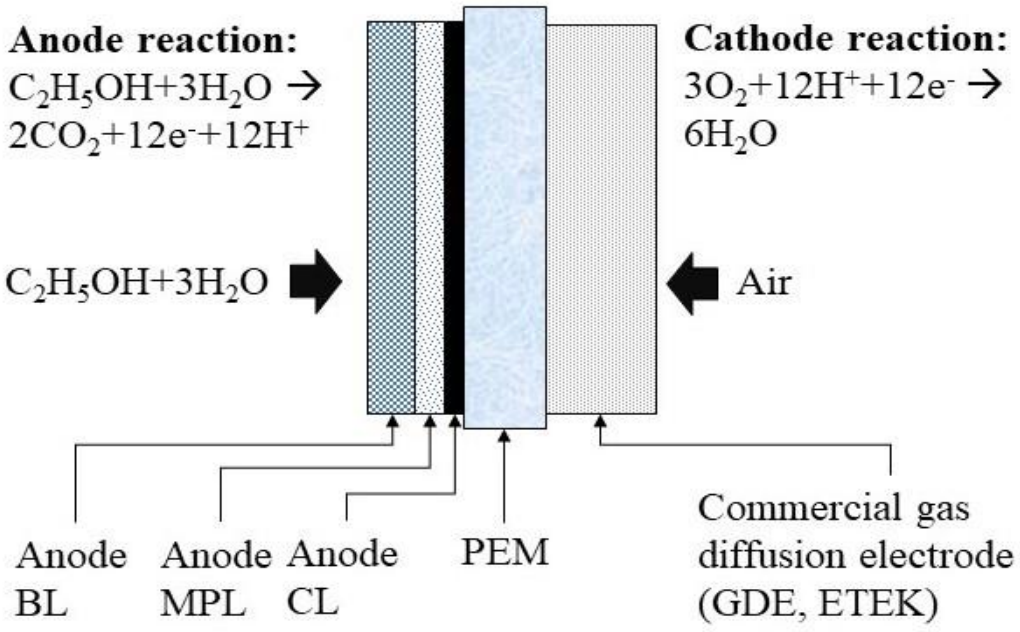

Figure 1 An illustration of the component of the MEA in a passive DEFC.

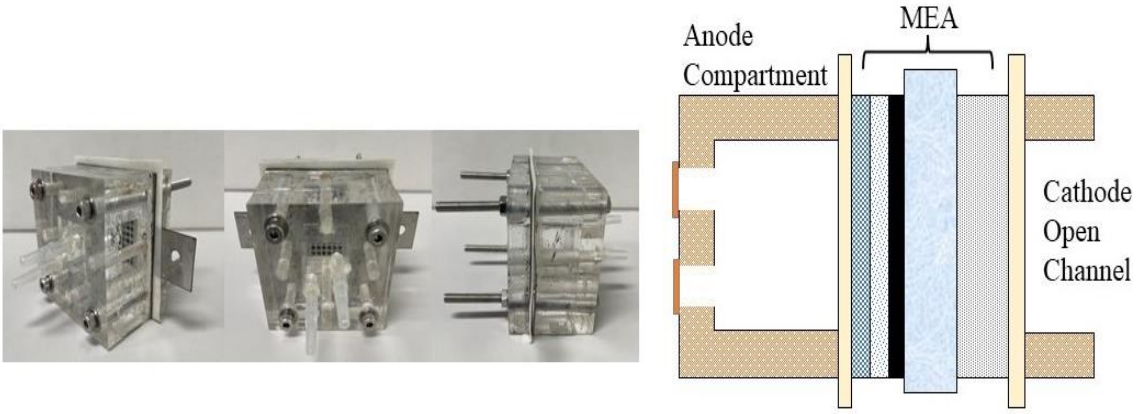

Figure 2 The assembled passive DEFC and custom-made single-cell stack.

Fuel cell characterization

An illustration of the apparatus arrangement is shown in **Figure 3** for the performance and characterization data that were collected using a potentiostat/galvanostat device (Metrohm Autolab, PGSTAT 302N, Utrecht, The Netherlands). To ensure a steady cell performance, a single-cell stack was initially operated continuously for 4 h. During this time, it was provided with a 1 M ethanol solution flowing at a rate of 1 mL·min^{-1} at the anode, while ambient air at room temperature (25 ºC) and atmospheric pressure was employed at the cathode open channel. Afterward, various characterization techniques were employed as follows.

In full-cell measurements, the anode compartment held an ethanol solution as the working electrode (WE), while the cathode was exposed to ambient air, serving as both the reference electrode (RE) and counter electrode (CE). Full-cell polarization evaluations were conducted using potentiodynamic mode over a range extending from the open circuit voltage (OCV) down to a low voltage of 0.1 V, employing a scanning rate of 10 mV·s^{-1} and a time interval of 10 seconds. Full-cell EIS measurements were conducted with a potentiostatic mode of 0.3 V, an amplitude of 30 mV, a frequency range of 1 kHz to 0.01 Hz, and 10 points per frequency decade. For a measurement of current variation with time measurement, it was controlled at the constant voltage of 0.3 V for 20 min and observed the corresponding cell current densities.

In the case of half-cell anode measurement with a slightly modified measurement, the anode employed an ethanol solution as the working electrode (WE), while the cathode employed hydrogen gas at a flow rate of 100 mL·min^{-1}, performing the dual functions of the dynamic hydrogen electrode (DHE) and counter electrode (CE), as suggested in the literature [25]. In this manner, half-cell polarization measurements were conducted in a potentiodynamic mode, covering a voltage range from 0 V to 0.6 V versus DHE.

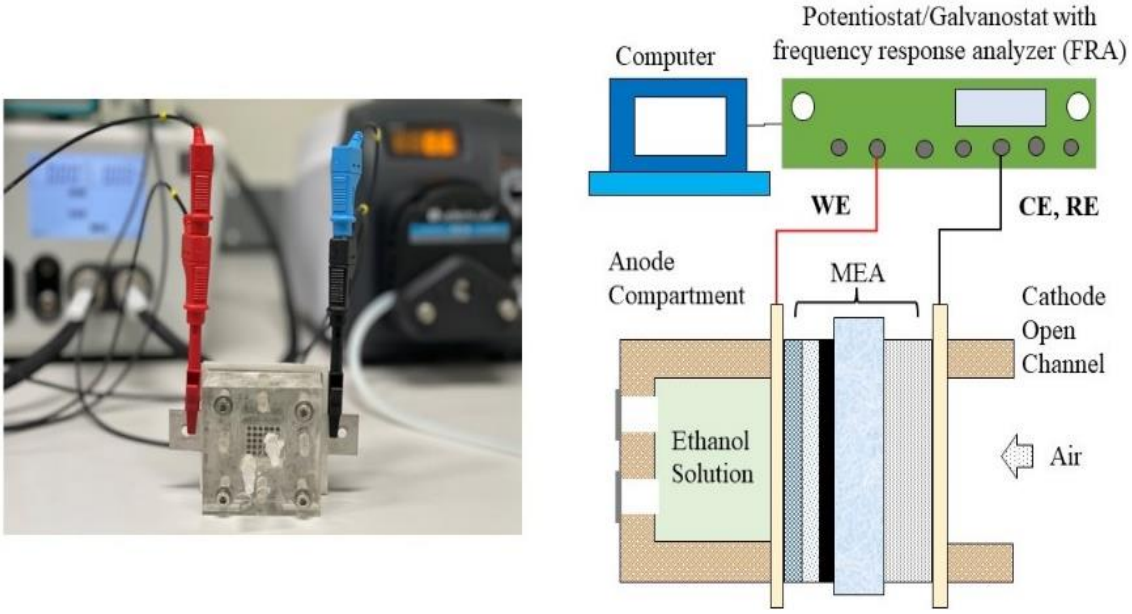

Figure 3 A schematic diagram of the experiment set-up.

Results and discussion

Full-cell polarization

The polarization and power density curves of passive DEFCs, employing 5 different anode DLs (as can be detailed in **Table 1**) and varying ethanol feed concentrations (1 to 6 M), are shown in **Figure 4**. The corresponding maximum power density data for each DL and concentration are presented in **Figure 5**. It is seen that the adoption of CC as an anode DL over CP resulted in the most significant improvements in cell performance. The performance of the cell with CP (ranging from 0.383 to 0.590 mW·cm^{-2}) was lower than that with CC_A (ranging from 0.421 to 0.772 mW·cm^{-2}). Compared to the highest value, the maximum power density of the cell using CC (CC_A) was improved by 30.83 % compared to that of the cell using CP, which is consistent with previous DMFC work that reported improvements of 48.82 % [13], 32 % [5],

and 9.1 % [7]. The primary reasons for this could be their higher porosity and thickness levels. Particularly in terms of porosity, CC is more porous than CP, which improves the diffusion mechanism for transporting fuel solution from the reservoir to the anode CL. The reduced porosity of CP limited the quantity of fuel solution reaching the anode CL, resulting in a decrease not only in the fuel crossover rate through the membrane but also in the rate of fuel oxidation due to an insufficiency of fuel molecules at the anode CL [5,7].

When using CC as a single-layer anode DL, in the low ethanol concentration range (1 to 4 M), the performance of the cell with CC_B (ranging between 0.532 and 0.661 $mW \cdot cm^{-2}$) appeared to be higher than the one with CC_A (ranging from 0.421 to 0.531 $mW \cdot cm^{-2}$). This finding revealed that DL wettability had an impact on the ethanol transport since the CC_B with hydrophobicity surface could minimize ethanol transport to the anode CL, which would lower the amount of ethanol crossover through the membrane to the cathode electrode, leading to higher cell performance. Contradictory, at higher ethanol concentrations (above 4 M), the performance of the cell with CC_B (ranging from 0.661 down to 0.657 $mW \cdot cm^{-2}$) was lower than that with CC_A (ranging from 0.531 to 0.772 $mW \cdot cm^{-2}$). It was believed that, while the ethanol oxidation reaction at a higher concentration, producing higher current densities, required a greater ethanol transport rate to the anode CL, there was not enough ethanol at the anode CL because the hydrophobic nature of the CC_B hindered ethanol transport.

While it was expected that the cell with the dual-layer structure of the DLs would offer better mass transport improvements, the cell performance with a CC_MPL_A (ranging from 0.384 to 0.617 $mW \cdot cm^{-2}$) was almost at a similar level to those with a single-layer anode DL (the cell with CC_A and CC_B) across the entire range of ethanol concentrations. Although the MPL could enhance ethanol utilization by ensuring a uniform distribution of ethanol on the anode electrode [5,13], the wettability of MPL proved unsuitable for balancing the mass transfer of ethanol. The hydrophilic nature of the Nafion ionomer in the MPL facilitated the crossing of the ethanol solution through the membrane to the cathode CL, promoting the crossover and water flooding effect, and contributing to the decrease of cell performance [26]. For this reason, the cell with CC_MPL_A could not outperform the cells using a single-layer anode DL. On the other hand, the cell equipped with a CC_MPL_B provided the best maximum power densities (ranging between 0.756 and 0.887 $mW \cdot cm^{-2}$) throughout the entire range of ethanol feed concentrations (1 to 6 M). It was expected that the balanced management of ethanol and water transport was achieved, which resulted in reduced activation resistance at both the anode and cathode electrodes. CC_MPL_B could offer not only a homogeneous distribution of reactants at the anode electrode due to the presence of MPL but also decrease the ethanol crossover rate to the cathode CL.

It is important to notice that each cell had an optimum ethanol feed concentration that corresponds to the best cell performance. The cells with CC_B and CC_MPL_A exhibited their best performance at a concentration of 4 M. The cells with CP and CC_MPL_B displayed their best performance at a concentration of 5 M. The cell with CC_A performed the best at an ethanol concentration of 6 M. Higher ethanol concentrations led to a significant decline in cell performance. The reason was that, at improper ethanol feed concentration levels, there is an imbalance in the competition between the benefit of oxidation reaction enhancement and the unfavorable effects of crossover [5,23]. Additionally, when considering cell operation at the optimum ethanol feed concentration, the cell performance could be improved by applying the appropriate DL. The best cell in our study (the one with CC_MPL_B) exhibited a maximum power density 14.96 % higher than that of the cell using CC without MPL (CC_A). However, it was observed that the percentage of improvement in this study was considerably lower than that reported in DMFC research, which showed improvements of 58.73 % [13] and 184.85 % [5]. This finding proves the difference in the kinetic reaction between DMFC and DEFC, which could influence their distinct mass transport characteristics. In the next section, we employed EIS and half-cell polarization to investigate the impact of anode DLs on individual cell resistance and prove the cell performance behavior.

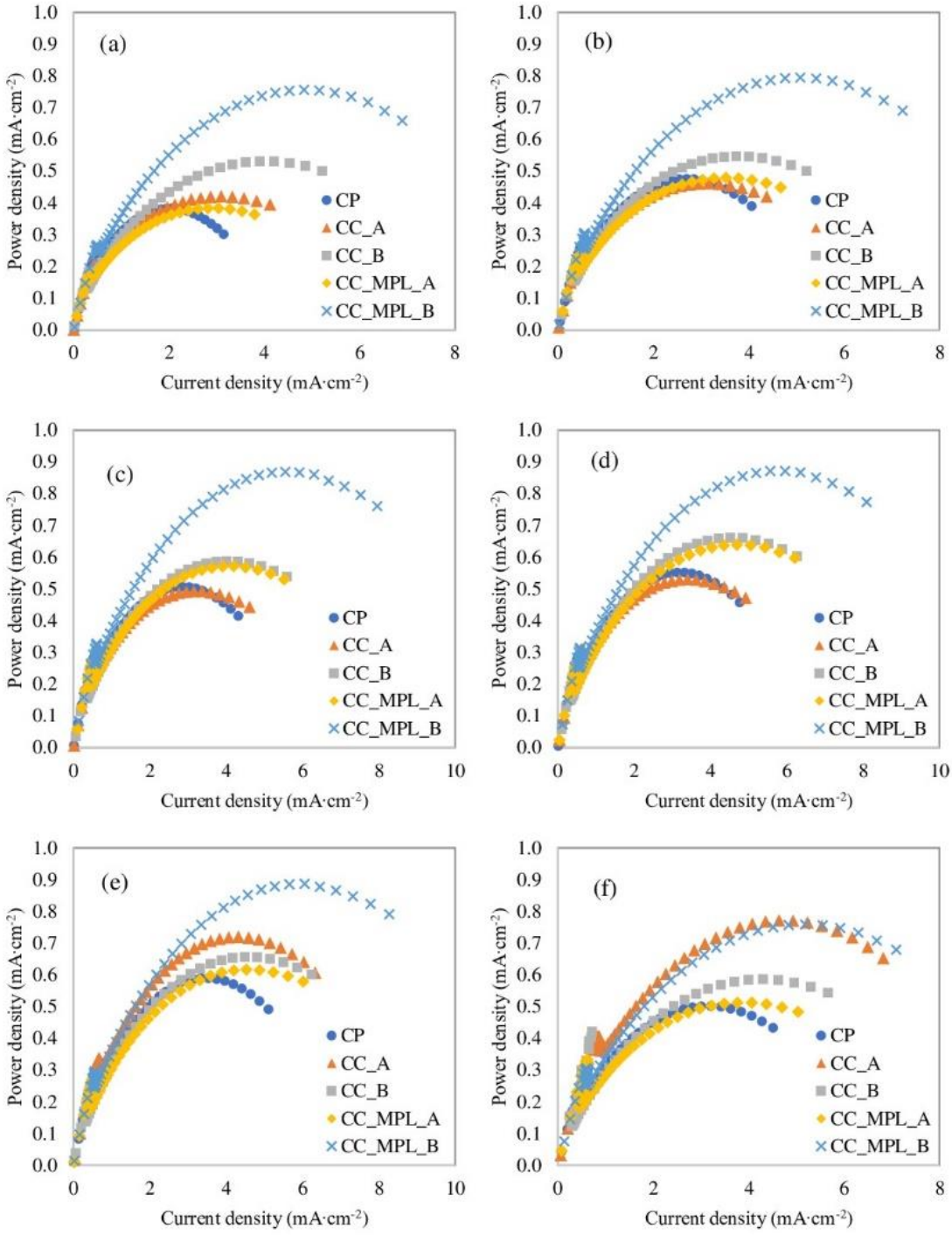

Figure 4 Power density curves for passive DEFCs with various anode DLs at concentrations of (a) 1 M, (b) 2 M, (c) 3 M, (d) 4 M, (e) 5 M, and (f) 6 M ethanol solution.

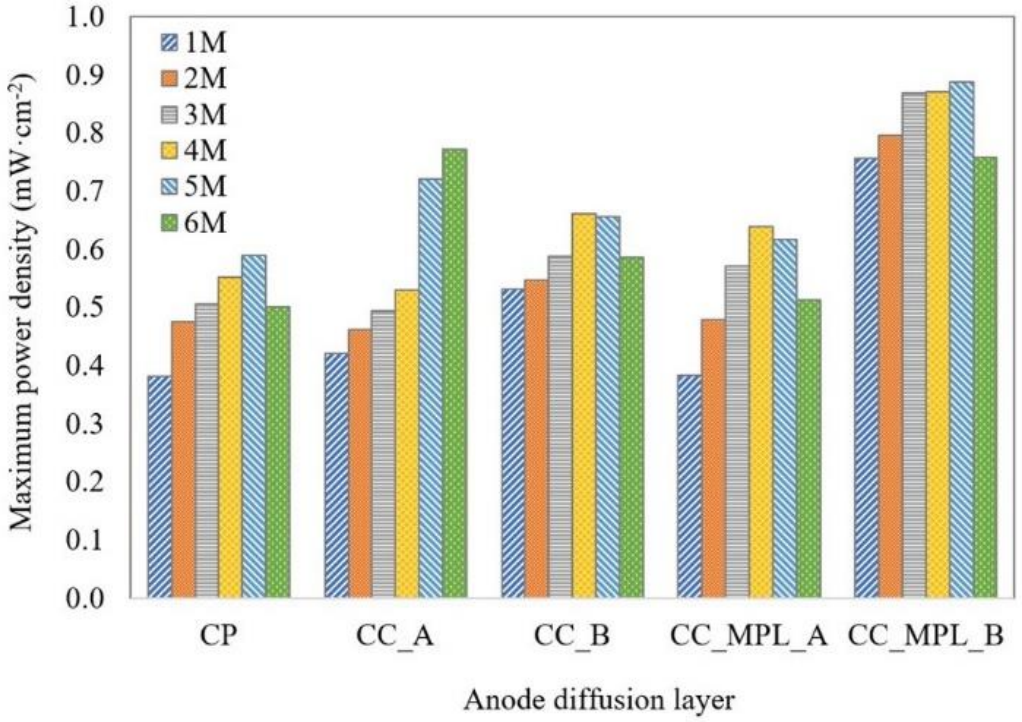

Figure 5 Summary of maximum power densities for passive DEFCs with the different DLs at various ethanol solution concentrations.

EIS measurement

The EIS technique offers important information on the overall performance of the passive liquid feed fuel cell as well as the behavior of the cell as it is affected by operating conditions and components [19]. In-situ electrochemical impedance spectroscopy (EIS) was conducted in full-cell mode to simultaneously understand the mechanism of the resistance at both anode and cathode electrodes. **Figure 6** shows the related impedance spectra (Nyquist plots) and a modified equivalent circuit used for fitting, developed from the models in the literature [27-29]. The following explanations provide the definitions of each parameter: W stands for the Warburg component; and L stands for the inductance produced by the conducting cables of an experiment. The cell ohmic resistance is represented by the R_{ohm}. The terms R_A and R_C represent the charge transfer resistance of the anode and cathode side, respectively. CPE_A and CPE_C record the capacitive behavior that illustrates the non-uniformity and roughness of the anode and cathode electrodes, respectively. The fitting parameters for the equivalent circuit model were obtained by fitting the experimental data and the important parameters, including R_{ohm}, R_A, and R_C for each cell, are summarized for comparison in **Figures 7** to **9**, respectively.

The discussion on R_{ohm} was initiated to explain the impact of DLs on cell ohmic resistance. The results indicated that, at low ethanol concentrations (1 to 4 M), R_{ohm} of the cell with CP (ranging from 1.327 to 1.512 Ω) was lower than that of CC_A (ranging from 1.859 to 1.640 Ω) due to the higher electronic conductivity and thinner structure of CP compared to CC [5]. On the contrary, at higher concentrations (above 4 M), the R_{ohm} of the cell with CC_A (ranging from 1.475 to 1.269 Ω) decreased and was lower than that of CP (ranging from 1.494 to 1.547 Ω). This behavior was believed due to, at a high ethanol feed concentration, the higher porosity in CC became more saturated with the water [19], allowing for an increase in electrical conductivity and thereby reducing ohmic resistance. In addition, the cell with the dual-layer structure of the DLs (CC_MPL_A and CC_MPL_B) seemed to have a lower R_{ohm} (decreased down to approximately 1 Ω), attributed to the fact that the presence of MPL could modify surface roughness, contributing to the improvement of surface attachment between the anode CL and anode BL [30]. However, the impact of R_{ohm} did not dominate the cell performance. It seemed that the main factor influencing cell performance was the activation resistance of the anode and cathode (R_A and R_C) which was discussed in detail below.

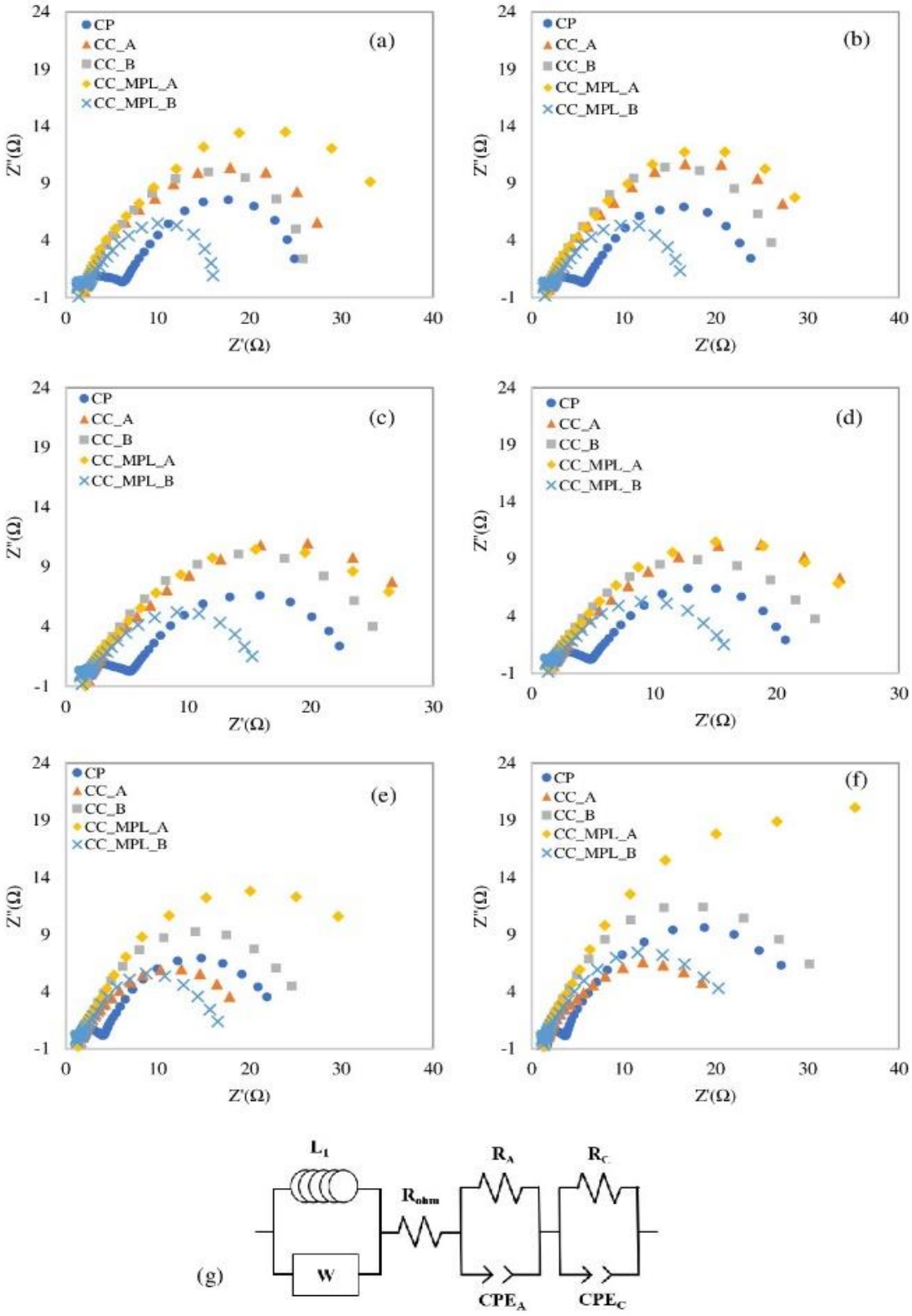

Figure 6 Electrochemical impedance spectra for passive DEFCs with different anode DLs at an ethanol solution concentration of (a) 1 M, (b) 2 M, (c) 3 M, (d) 4 M, (e) 5 M, (f) 6 M, and (g) equivalent circuit for the EIS analysis.

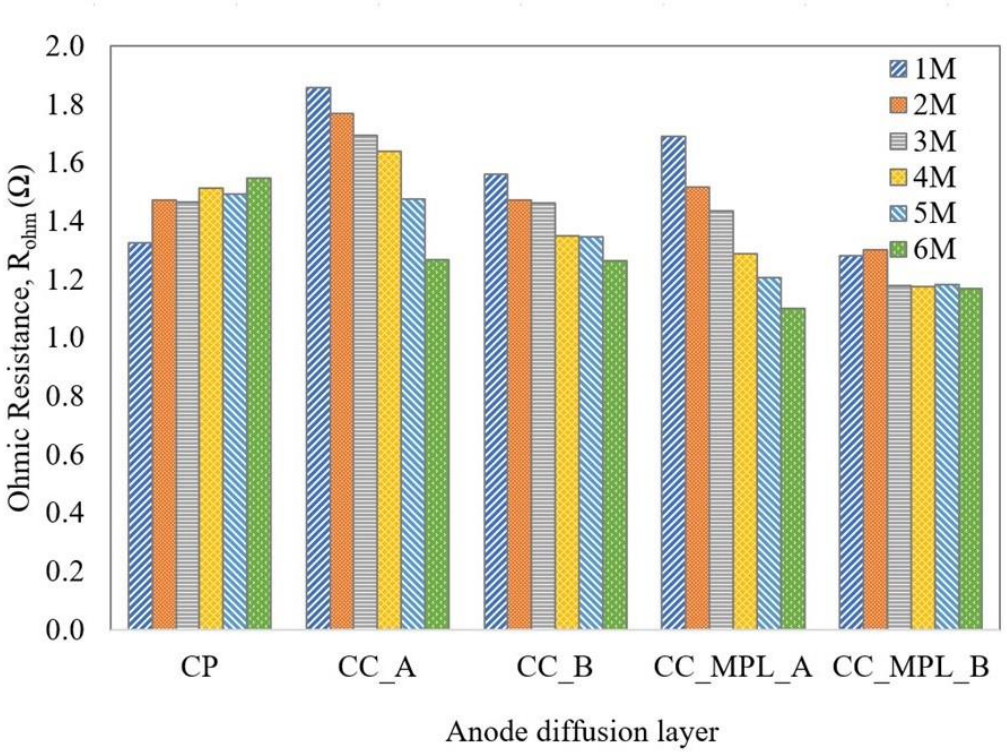

Figure 7 Summary of R_{ohm} from the fitting parameters for passive DEFCs with the different DLs at various ethanol solution concentrations.

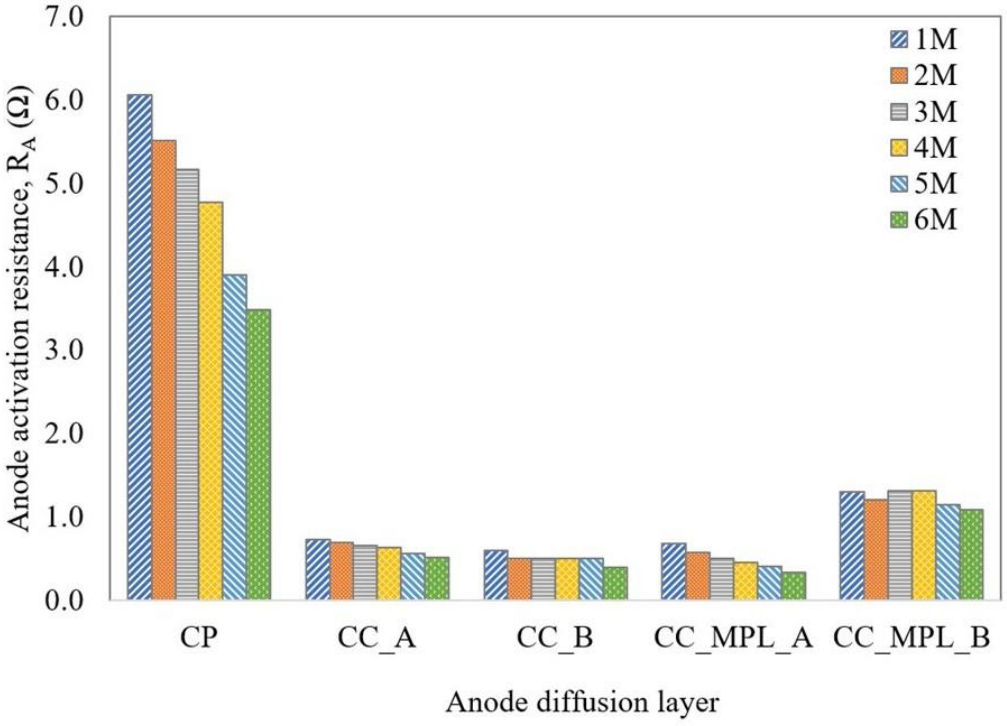

Figure 8 Summary of R_A from the fitting parameters for passive DEFCs with the different DLs at various ethanol solution concentrations.

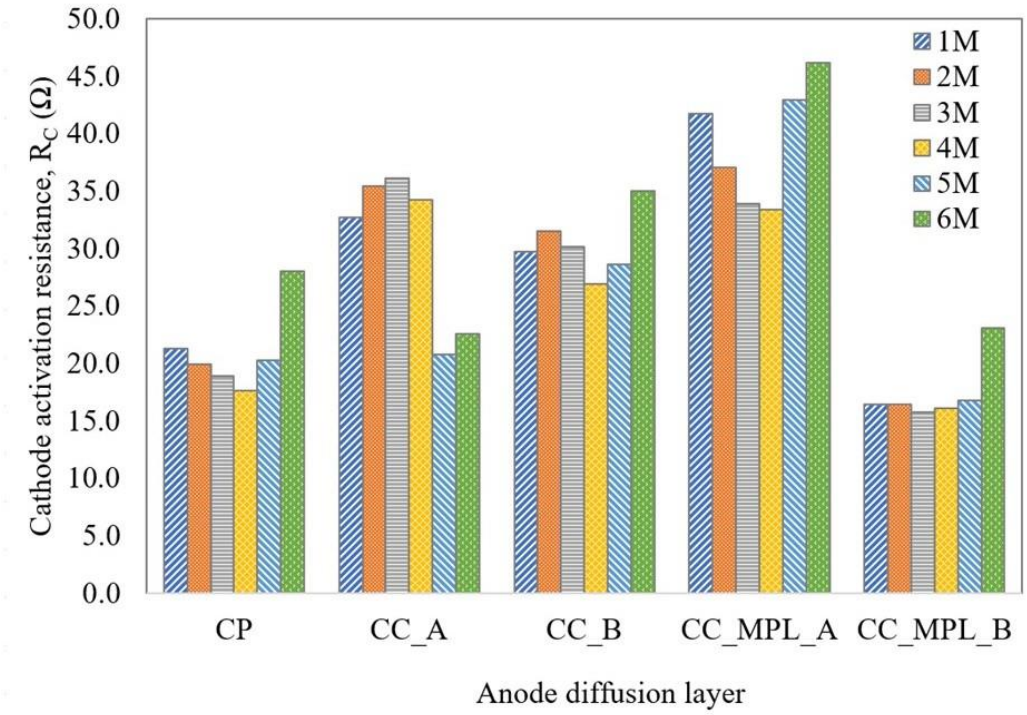

Figure 9 Summary of R_C from the fitting parameters for passive DEFCs with the different DLs at various ethanol solution concentrations.

The cell with CP exhibited the highest R_A (ranging from 6.066 to 3.489 Ω), whereas it had a relatively low R_C (fluctuating between 17.642 and 28.054 Ω). Based on literature reports [5,7], this was considered to be the effect of lower porosity in CP, which limits the quantity of ethanol solution that can reach the anode CL and leads to the decreased ethanol crossover to the cathode CL. An extreme limitation of the ethanol solution resulted in an insufficient amount of ethanol for the ethanol oxidation reaction, especially during high current discharge, which was expected to account for the incredibly poor cell performance. The R_A of the cell with CC_A (ranging from 0.730 to 0.508 Ω) was close to that of CC_B (ranging from 0.596 to 0.397 Ω), indicating a similar anode activation loss. Both cells with CC_A and CC_B exhibited low R_A due to the absence of an MPL in their DLs, enabling efficient ethanol transfer from the anode compartment to the anode CL. The difference was clearly shown through the R_C behavior. At low ethanol concentrations (1 to 4 M), the cell with CC_B displayed a lower R_C (varying between 26.930 and 31.529 Ω) compared to the cell with CC_A (fluctuating between 32.746 and 36.112 Ω). The hydrophobic surface of CC_B was identified as a factor that reduced ethanol crossover to the cathode electrode, resulting in lower cathode activation loss and contributing to higher cell performance. In contrast, at higher ethanol concentrations (above 4 M), the cell with CC_A exhibited a sudden decrease in R_C (ranging from 20.781 to 22.577 Ω) compared to that of the cell with CC_B (ranging from 28.645 to 35.046 Ω). It could be explained that, at elevated ethanol concentrations, the oxidation reaction required more ethanol molecules for higher current densities. The cell with CC_A, facilitating effective anode mass transport, played a crucial role in utilizing increased ethanol amounts, reducing the ethanol crossover effect at the cathode CL and thereby enhancing overall cell performance.

Considering the cell with the dual-layer structure of the DLs, the R_A of the cell with CC_MPL_A (ranging from 0.675 to 0.331 Ω) was at a low level, similar to that of the cells with CC_A and CC_B. The hydrophilic nature of MPL improved ethanol distribution and facilitated ethanol mass transfer at the anode electrode, resulting in a relatively low anode activation resistance. Unfortunately, this scenario could lead to an increased rate of ethanol crossover to the cathode, causing an adverse mixed potential effect that obviously elevated R_C to reach the highest level (ranging from 33.443 to 66.173 Ω). The adverse impact of crossover outweighed the positive effect of an improved mass transfer at the anode, resulting in diminished cell performance.

Noteworthy, according to the cell with CC_MPL_B, which offered the best cell performance at all ethanol concentrations, the R_A was within a moderate range, fluctuating from 1.089 to 1.308 Ω. It was understood that its anode MPL, with hydrophobicity, not only contributed to improving the distribution of ethanol within the anode CL but also diminished the mass transport of ethanol to the anode CL. These 2 opposing effects combined to result in an acceptable level of R_A. Furthermore, the decreased ethanol mass transport at the anode was beneficial in preventing ethanol crossover to the cathode, contributing to the achievement of a remarkably low R_C (ranging between 15.775 and 23.105 Ω). This was essential for sustaining the oxygen reduction reaction at the cathode, leading to excellent overall cell performance.

Anode half-cell polarization

The anode potentials of the cells with various DLs were determined utilizing the cathode as a DHE, as shown in **Figure 10**. The anode half-cell limiting current densities, considered at 0.6 V vs DHE, were chosen as the comparative data. **Figure 11** provides a summary of the anode half-cell limiting current densities that were determined at various ethanol concentrations and DLs. The results presented that the cell with CP had a relatively small anode-limiting current density (ranging from 7.217 to 12.750 $mA \cdot cm^{-2}$), in accordance with the high anode activation resistance attributed to the limitation of ethanol solution reaching the anode CL. The cell with CC_B obtained an anode-limiting current density (ranging from 8.955 to 15.295 $mA \cdot cm^{-2}$) at a low level, similar to that of the cell with CP. This evidence corroborates the role of the hydrophobic surface of CC_B, which prevents ethanol transport to the anode CL. The cell with CC_A exhibited the highest anode half-cell limiting current density (ranging from 13.837 to 20.514 $mA \cdot cm^{-2}$) across a range of ethanol feed concentrations. It could be confirmed that CC A, with no obstacles impeding ethanol mass transport, promoted a large amount of ethanol transfer to the anode CL. However, the overall cell performance was not improved because an excessive transport of ethanol permeated across the membrane, forming a mixed potential at the cathode, which led to a decreased cell performance.

Regarding the cell using CC_MPL_B, the anode-limiting current density was found to be at a moderate level (ranging from 13.275 to 18.634 $mA \cdot cm^{-2}$), confirming that CC_MPL_B effectively distributed ethanol solution transport in the anode electrode, leading to enhanced oxidation reactions across the entire voltage range. Importantly, the hydrophobic characteristic of MPL played a crucial role in minimizing ethanol crossover to the cathode electrode, leading to outstanding overall cell performance. Remarkably, it was found that the anode-limiting current density result from the cell using CC_MPL_A should be specifically clarified. In fact, the DL with hydrophilic characteristics in the cell with CC_MPL_A would promote the ethanol transport from the anode reservoir to the anode CL, resulting in an increased anode-limiting current density and subsequently reduced anode activation resistance, as explained in the prior section (EIS experiment). Contrary to expectations, this experimental result illustrated that the cell with CC_MPL_A significantly hindered ethanol transport to the anode CL, leading to a reduced anode-limiting current density. The result showed that the cell with CC_MPL_A provided the lowest anode-limiting current density (ranging from 6.873 to 11.548 $mA \cdot cm^{-2}$). This finding was believed to be a result of the Nafion ionomer in the MPL encountering swelling behavior at higher voltage (relating to high ethanol oxidation reaction rate) [26,31], which acted as a barrier, preventing ethanol transport to the anode CL and eventually reducing the anode-limiting current density. Hence, the cell with CC_MPL_A could not maintain suitable ethanol transportation for the entire range of the cell voltage operation, resulting in poor cell performance.

Likewise, as shown in **Figure 11**, there was an upward trend in the anode limiting current for every cell with the increase in ethanol feed concentration. In comparison to **Figure 5**, which illustrated the overall cell performance, each cell had an optimal ethanol feed concentration associated with the best cell performance. In other words, half-cell performance increased with the rise in ethanol concentration, while overall cell performance was enhanced up to the optimal concentration and declined thereafter. This confirmed that the decline in cell performance could be attributed to the dominant negative impact of the increased ethanol crossover rate at high ethanol feed concentrations, leading to the formation of a mixed potential and an increased cathode activation resistance.

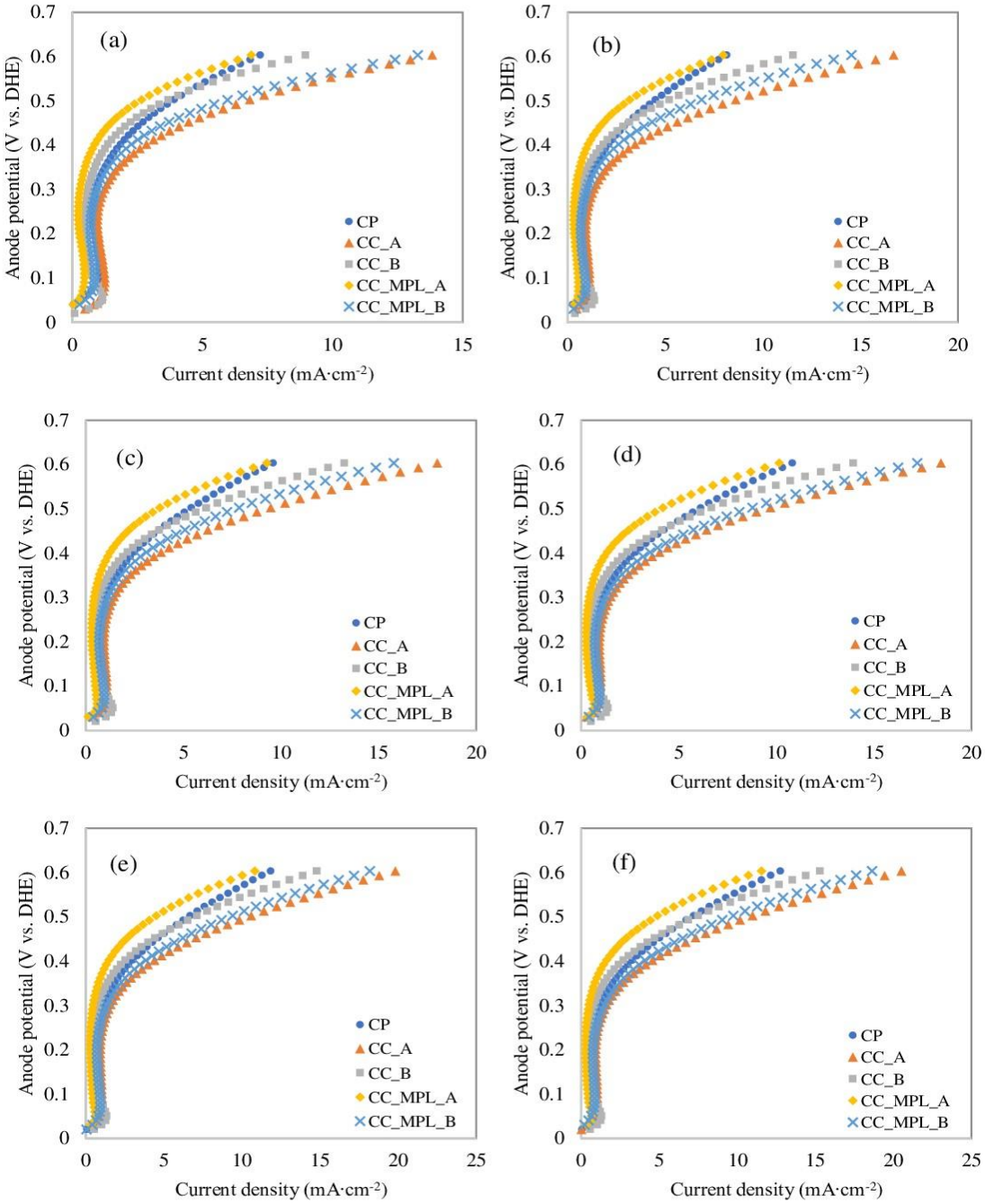

Figure 10 Anode half-cell polarizations for passive DEFCs with various anode DLs at ethanol solution concentrations of (a) 1 M, (b) 2 M, (c) 3 M, (d) 4 M, (e) 5 M, (f) 6 M, and (g) equivalent circuit for the EIS analysis.

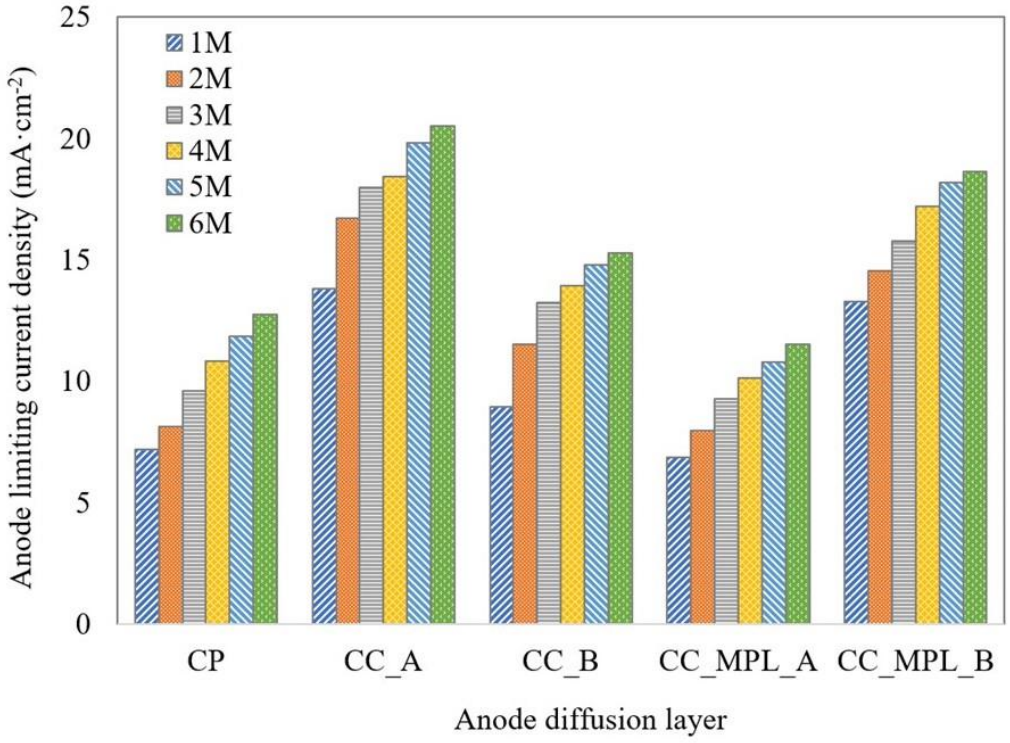

Figure 11 Summary of anode half-cell limiting current densities for passive DEFCs with various ethanol solutions and varied DLs.

Current variation with time measurement

This experiment was conducted to better understand the effect of mass transport behavior on cell performance over time. The experiment was carried out by maintaining constant voltages at 0.3 V, and the cell current densities were collected during testing time. **Figure 12** displays the time-dependent variations in current densities for passive DEFCs equipped with different anode DLs and varying concentrations of ethanol solution. The current densities observed at the final point (at 20 min) for each cell were assumed to represent long-term cell performance and are summarized in **Figure 13**. The decay in current density over time was related to an increase in mass transport resistance to the anode CL, becoming evident as time progressed. This was a consequence of the gradual buildup of intermediate reaction products, including CO, acetic acid, and acetaldehyde, at the anode CL during continuous current discharge [32]. Fortunately, it was realized that liquid water flooding within the cathode electrode was not strong in any of the cells, as indicated by the absence of noticeable fluctuations in current densities during voltage discharges, as reported in a prior study [26].

Due to the fact that a longer time progression can highlight mass transport behavior and thereby influence long-term cell performance, there is a slight difference in long-term performance for each cell compared to full-cell performance. The function of DL related to mass transport management, such as the prevention of crossover, would be more essential in enhancing and stabilizing cell performance. For this reason, the long-term performance of the cell with CP became more notable at low ethanol concentrations (1 to 4 M), ranging between 0.648 and 0.679 $mA \cdot cm^{-2}$. Nevertheless, it experienced a sudden decrease when employing elevated ethanol concentrations (above 4 M), which proved excessive to maintain the crossover effect. This pattern was also observed in the cell with CC_B, but it exhibited lower long-term performance, ranging from 0.480 to 0.190 $mA \cdot cm^{-2}$, attributed to a severe hydrophobic nature hindering ethanol transport to the anode CL. Surprisingly, the cell with CC_A demonstrated acceptable long-term performance, effectively counteracting the detrimental effects of ethanol crossover over time. This resulted in a moderate value for the long-term performance ranging between 0.534 and 0.724 $mA \cdot cm^{-2}$ and enabled the cell to function effectively even at higher ethanol feed concentrations (up to 5 M). The result also illustrated that the long-term performance of the cell with CC_MPL_A (ranging from 0.318 to 0.085 $mA \cdot cm^{-2}$) was the lowest, primarily due to its ineffective mass transport management. This is a result of

experiencing both extremely high mass transport at low reaction rates and the prevention of ethanol transport due to Nafion swelling at high reaction rates. Importantly, when considering the cell with CC_MPL_B, it demonstrated successful enhancement in long-term performance, operating at its highest level ranging from 0.942 to 0.422 $mA \cdot cm^{-2}$. This improvement strongly supports the finding that CC_MPL_B, as an anode DL, provided effective mass transport management at the anode and reasonable encouragement to reduce ethanol crossover at the cathode.

It was mentioned that the majority of long-term cell performances for each cell approached the highest values at relatively low ethanol feed concentrations (1 to 3 M), in contrast to the optimum ethanol feed concentration (4 to 6 M) corresponding to the highest maximum power density, as seen in the full-cell polarization test depicted in **Figure 5**. The decrease in the optimal ethanol concentration for the best long-term performance was ascribed to the growing accumulation of both intermediate reactions at the anode and ethanol crossover at the cathode during extended testing periods. As a result, there was a decrease in the overall performance of the cell, especially when generating high current density with elevated ethanol concentrations.

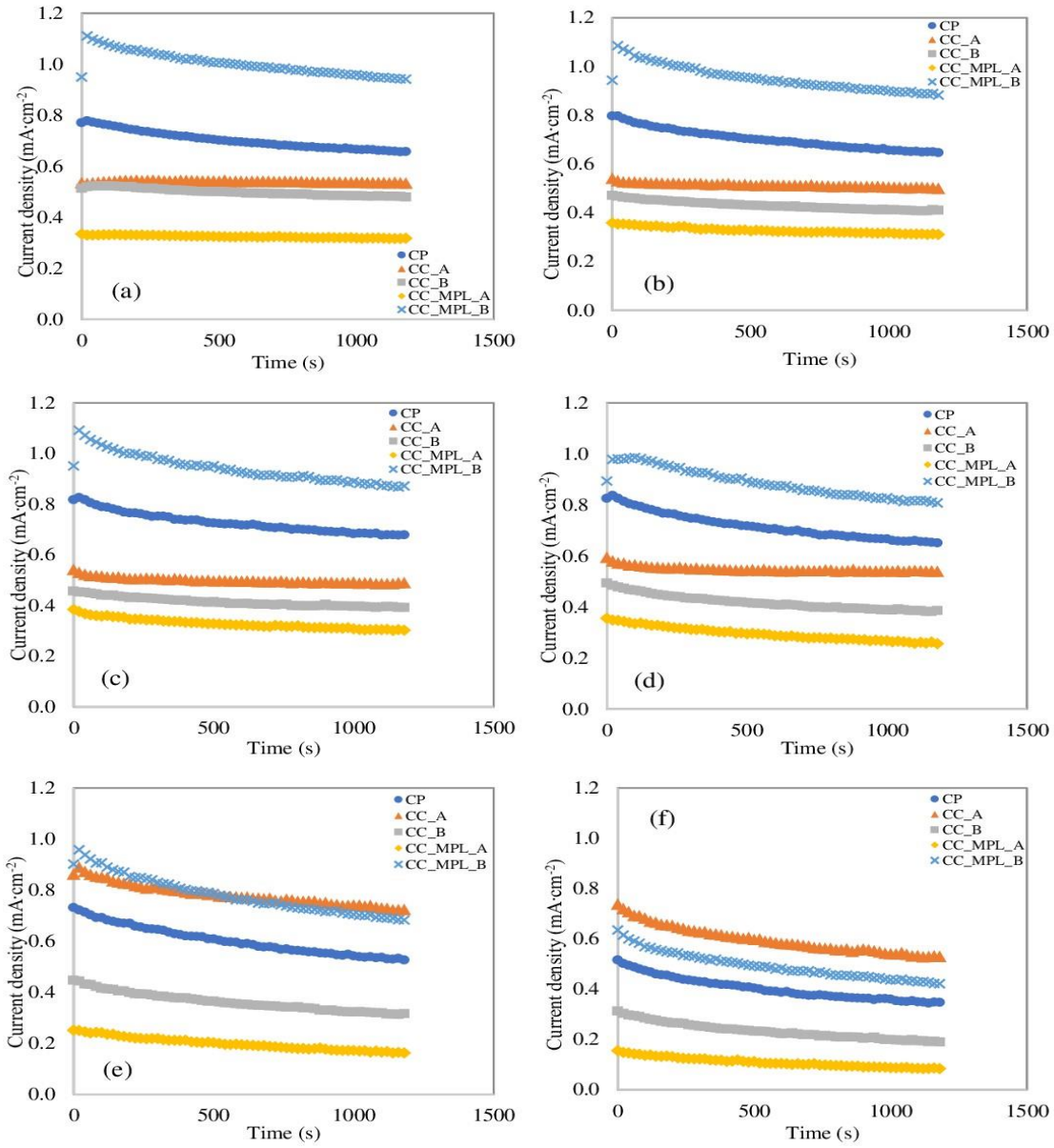

Figure 12 Current densities variable with time for passive DEFCs with various anode DLs at concentrations of ethanol solution of (a) 1 M, (b) 2 M, (c) 3 M, (d) 4 M, (e) 5 M, (f) 6 M.

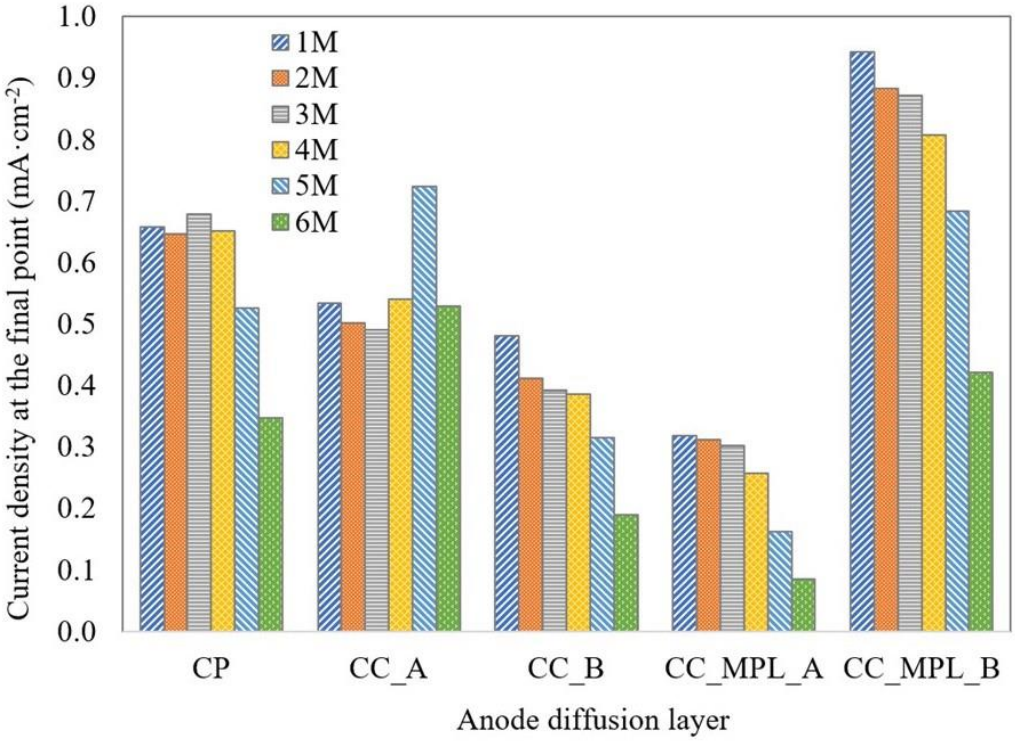

Figure 13 Summary of the final point of the current densities corresponding to the current variation with time measurement for passive DEFCs with the different DLs at various ethanol solutions.

Conclusions

In this study, the effect of various DLs made of readily available commercial materials on the performance of the cell was examined in passive DEFCs with a range of ethanol feed concentrations. Different anode DL architectures were created to achieve the promised power outputs needed for the passive DEFC application. There were several methods used for characterizing the samples, including full-cell polarization, full-cell EIS, half-cell polarization, and current variation with time measurement.

The significant performance enhancements were attributed to the use of CC as an anode DL instead of CP. This is primarily due to its higher porosity and thickness, leading to the improved diffusion of ethanol. The dual-layer DL structure, incorporating MPL, provided superior cell performance by enhancing ethanol utilization through a more uniform reactant distribution in the electrode, thereby reducing anode activation resistance and simultaneously ethanol flux through the membrane.

The cell with CC_MPL_B achieved the best performance at a maximum power density of 0.887 $mW \cdot cm^{-2}$ at the optimal ethanol feed concentration of 5 M due to the enhanced ethanol and water transport management at both the anode and cathode electrodes. The superior performance could be confirmed by the supported evidence from various characteristics, as discussed below:

1) EIS results showed that the cell with CC_MPL_B, which exhibited the best cell performance across all ethanol concentrations, displayed an average R_A due to the hydrophobic nature of MPL, slightly reducing ethanol transport to the anode CL. At the same time, the cell showed the lowest R_C, which could prove the prevention of crossover to the cathode.

2) In the anode half-cell polarization test, the cell with CC_MPL_B displayed the second-highest limiting current density, demonstrating its effectiveness in facilitating ethanol and water transport at the anode, thereby improving oxidation reactions.

3) In the experiment measuring current variation over time, the cell with CC_MPL_B could maintain a higher level of current density compared to other cells, which corresponded to effective mass transport management at the anode and a robust capability to reduce ethanol crossover at the cathode.

In summary, to enhance cell performance, the ideal design of the anode DL should prioritize achieving a balance by simultaneously improving the anode reaction rate and reasonably preventing ethanol crossover.

Acknowledgements

This research was funded by the National Science, Research and Innovation Fund (NSRF), and King Mongkut's University of Technology North Bangkok with Contract no. KMUTNB-FF-65-43 and the author would like to acknowledge the Faculty of Science, Energy and Environment (SCIEE), King Mongkut's University of Technology North Bangkok (Rayong campus), Thailand for their support of the facility.

References

[1] K Elsaid, S Abdelfatah, AMA Elabsir, RJ Hassiba, ZK Ghouri and L Vechot. Direct alcohol fuel cells: Assessment of the fuel's safety and health aspects. *Int. J. Hydrogen Energ.* 2021; **46**, 30658-68.

[2] MHD Sá, AMFR Pinto and VB Oliveira. Passive small direct alcohol fuel cells for low-power portable applications: Assessment based on innovative increments since 2018. *Energies* 2022; **15**, 3787.

[3] DM Fadzillah, SK Kamarudin, MA Zainoodin and MS Masdar. Critical challenges in the system development of direct alcohol fuel cells as portable power supplies: An overview. *Int. J. Hydrogen Energ.* 2018; **44**, 3031-54.

[4] SS Munjewar, SB Thombre and RK Mallick. Approaches to overcome the barrier issues of passive direct methanol fuel cell - review. *Renew. Sust. Energ. Rev*. 2017; **67**, 1087-104.

[5] VB Oliveira, JP Pereira and AMFR Pinto. Effect of anode diffusion layer (GDL) on the performance of a passive direct methanol fuel cell (DMFC). *Int. J. Hydrogen Energ.* 2016; **41**, 19455-62.

[6] MA Abdelkareem, A Allagui, ET Sayed, EH Assad, Z Said and K Elsaid. Comparative analysis of liquid versus vapor-feed passive direct methanol fuel cells. *Renew. Energ.* 2019; **131**, 563-84.

[7] MA Abdelkareem, ET Sayed and N Nakagawa. Significance of diffusion layers on the performance of liquid and vapor feed passive direct methanol fuel cells. *Energy* 2020; **209**, 118492.

[8] KA Nagy, IY Tóth, G Ballai, ÁT Varga, I Szenti, D Sebők, J Kopniczky, B Hopp and Á Kukovecz. Wetting and evaporation on a carbon cloth type gas diffusion layer for passive direct alcohol fuel cells. *J. Mol. Liq*. 2020; **304**, 112698.

[9] T Yuan, J Yang, Y Wang, H Ding, X Li, L Liu and H Yang. Anodic diffusion layer with graphene-carbon nanotubes composite material for passive direct methanol fuel cell. *Electrochim Acta* 2014; **147**, 265-70.

[10] W Yuan, B Zhou, J Hu, J Deng, Z Zhang and Y Tang. Passive direct methanol fuel cell using woven carbon fiber fabric as mass transfer control medium. *Int. J. Hydrogen Energ.* 2015; **40**, 2326-33.

[11] BC Ong, SK Kamarudin, MS Masdar and UA Hasran. Applications of graphene nano-sheets as anode diffusion layers in passive direct methanol fuel cells (DMFC). *Int. J. Hydrogen Energ.* 2017; **42**, 9252-61.

[12] M Boni, SS Rao, GN Srinivasulu and ChV Narayana. Effect of anode gas diffusion layer thickness and porosity on the performance of passive direct methanol fuel cell. *Chem. Prod. Process Model*. 2019; **14**, 20190029.

[13] BA Braz, VB Oliveira and AMFR Pinto. Experimental evaluation of the effect of the anode diffusion layer properties on the performance of a passive direct methanol fuel cell. *Energies* 2020; **13**, 5198.

[14] MS Alias, SK Kamarudin, AM Zainoodin and MS Masdar. Structural mechanism investigation on methanol crossover and stability of a passive direct methanol fuel cell performance via modified micro-porous layer. *Int. J. Energ. Res*. 2021; **45**, 12928-43.

[15] SPS Badwal, S Giddey, A Kulkarni, J Goel and S Basu. Direct ethanol fuel cells for transport and stationary applications - A comprehensive review. *Appl. Energ*. 2015; **145**, 80-103.

[16] S Song, W Zhoua, Z Liang, R Cai, G Sun, Q Xin, V Stergiopoulos and P Tsiakaras. The effect of methanol and ethanol cross-over on the performance of PtRu/C-based anode DAFCs. *Appl. Catal. B Environ*. 2005; **55**, 65-72.

[17] N Fujiwara, Z Siroma, S Yamazaki, T Ioroi, H Senoh and K Yasuda. Direct ethanol fuel cells using an anion exchange membrane. *J. Power Sourc*. 2008; **185**, 621-6.

[18] N Shaari, SK Kamarudin, R Bahru, SH Osman and NAIM Ishak. Progress and challenges: Review for direct liquid fuel cell. *Int. J. Energ. Res*. 2021; **45**, 6644-88.

[19] BA Braz, CS Moreira, VB Oliveira and AMFR Pinto. Electrochemical impedance spectroscopy as a diagnostic tool for passive direct methanol fuel cells. *Energ. Rep*. 2022; **8**, 7964-5.
[20] F Jing, R Sun, S Wang, H Sun and G Sun. Effect of the anode structure on the stability of a direct methanol fuel cell. *Energ. Fuel* 2020; **34**, 3850-7.
[21] A Alrashidi and H Liu. Laser-peforated anode gas diffusion layers for direct methanol fuel cells. *Int. J. Hydrogen Energ*. 2021; **46**, 4622-9.
[22] M Haskul, AT Ulgen and A Doner. Fabrication and characterization of Ni modified TiO_2 electrode as anode material for direct methanol fuel cell. *Int. J. Hydrogen Energ*. 2020; **45**, 4860-74.
[23] H Wu, H Zhang, P Chen, J Guo, T Yuan, J Zheng and H Yang. Integrated anode structure for passive direct methanol fuel cells with neat methanol operation. *J. Power Sourc.* 2014; **248**, 1264-9.
[24] K Zuo and Z Yuan. Design and experimental analysis of a dual-cavity high-concentration adaptive passive micro direct methanol fuel cell. *Int. J. Energ. Res*. 2021; **45**, 5359-68.
[25] J Prabhuram, NN Krishnan, B Choi, TH Lim, HY Ha and SK Kim. Long-term durability test for direct methanol fuel cell made of hydrocarbon membrane. *Int. J. Hydrogen Energ*. 2010; **35**, 6924-33.
[26] F Liu and CY Wang. Water and methanol crossover in direct methanol fuel cells - effect of anode diffusion media. *Electrochim Acta* 2008; **53**, 5517-22.
[27] J Cao, M Chen, J Chen, S Wang, Z Zou, Z Li, DL Akins and H Yang. Double microporous layer cathode for membrane electrode assembly of passive direct methanol fuel cells. *Int. J. Hydrogen Energ*. 2010; **35**, 4622-9.
[28] J Cao, L Wang, L Songa, J Xu, H Wang, Z Chen, Q Huang and H Yang. Novel cathodal diffusion layer with mesoporous carbon for the passive direct methanol fuel cell. *Electrochim Acta* 2014; **118**, 163-8.
[29] P Ekdharmasuit, J Sapkitjakarn, P Sangwanangkool, A Bampenrat and H Sukkathanyawat. Performance study on cathode microporous layer using biomass activated carbon for passive direct ethanol fuel cell. *J. Ecol. Eng*. 2023, **24**, 214-24.
[30] VB Oliveira, DS Falcão, CM Rangel and AMFR Pinto. Water management in a passive direct methanol fuel cell. *Int. J. Energ. Res*. 2012, **37**, 991-1001.
[31] P Ekdharmasuit, A Therdthianwong and S Therdthianwong. The role of an anode microporous layer in direct ethanol fuel cells at different ethanol concentrations. *Int. J. Hydrogen Energ*. 2014; **39**, 1775-82.
[32] P Ekdharmasuit, A Therdthianwong and S Therdthianwong. Anode structure design for generating high stable power output for direct ethanol fuel cells. *Fuel* 2013; **113**, 69-76.